Hindawi Publishing Corporation
Mathematical Problems in Engineering
Volume 2012, Article ID 479087, 18 pages
doi:10.1155/2012/479087

Research Article

Williamson Fluid Model for the Peristaltic Flow of Chyme in Small Intestine

Sohail Nadeem,[1] Sadaf Ashiq,[1] and Mohamed Ali[2]

[1] *Department of Mathematics, Quaid-i-Azam University, Islamabad 45320, Pakistan*
[2] *Department of Mechanical Engineering, King Saud University, Riyadh 11451, Saudi Arabia*

Correspondence should be addressed to Sohail Nadeem, snqau@hotmail.com

Received 21 September 2011; Revised 24 December 2011; Accepted 2 January 2012

Academic Editor: Angelo Luongo

Mathematical model for the peristaltic flow of chyme in small intestine along with inserted endoscope is considered. Here, chyme is treated as Williamson fluid, and the flow is considered between the annular region formed by two concentric tubes (i.e., outer tube as small intestine and inner tube as endoscope). Flow is induced by two sinusoidal peristaltic waves of different wave lengths, traveling down the intestinal wall with the same speed. The governing equations of Williamson fluid in cylindrical coordinates have been modeled. The resulting nonlinear momentum equations are simplified using long wavelength and low Reynolds number approximations. The resulting problem is solved using regular perturbation method in terms of a variant of Weissenberg number W_e. The numerical solution of the problem is also computed by using shooting method, and comparison of results of both solutions for velocity field is presented. The expressions for axial velocity, frictional force, pressure rise, stream function, and axial pressure gradient are obtained, and the effects of various emerging parameters on the flow characteristics are illustrated graphically. Furthermore, the streamlines pattern is plotted, and it is observed that trapping occurs, and the size of the trapped bolus varies with varying embedded flow parameters.

1. Introduction

The object of this study is to investigate the flow induced by peristaltic action of chyme (treated as Williamson fluid) in small intestine with an inserted endoscope. Williamson fluid is characterized as a non-Newtonian fluid with shear thinning property (i.e., viscosity decreases with increasing rate of shear stress). Since many physiological fluids behave like a non-Newtonian fluid [1], so chyme in small intestine is assumed to behave like Williamson fluid. Peristaltic motion is one of the most characteristics fluid transport mechanism in many biological systems. It pumps the fluids against pressure rise. It involves involuntary movements of the longitudinal and circular muscles, primarily in the digestive tract

but occasionally in other hollow tubes of the body, that occur in progressive wavelike contractions. The waves can be short, local reflexes or long, continuous contractions that travel the whole length of the organ, depending upon their location and what initiates their action.

In human gastrointestinal tract, the peristaltic phenomenon plays a vital role throughout the digestion and absorption of food. The small intestine is the largest part of the gastrointestinal tract and is composed of the duodenum which is about one foot long, the jejunum (5–8 feet long), and the ileum (16–20 feet long). The rhythmic muscular action of the stomach wall (peristalsis) moves the chyme (partially digested mass of food) into the duodenum, the first section of the small intestine, where it stimulates the release of secretin, a hormone that increases the flow of pancreatic juice as well as bile and intestinal juices. Nutrients are absorbed throughout the small intestine. There are blood vessels and vessels contained a fluid called lymph inside the villi. Fat-soluble vitamins and fatty acids are absorbed into the lymph system. Glucose, amino acids, water-soluble vitamins, and minerals are absorbed into the blood vessels. The blood and lymph then carry the completely digested food throughout the body [2].

The endoscope effect on peristaltic motion occurs in many medical applications. Direct visualization of interior of the hollow gastrointestinal organs is one of the most powerful diagnostic and therapeutic modalities in modern medicine. A flexible tube called an endoscope is used to view different parts of the digestive tract. The tube contains several channels along its length. The different channels are used to transmit light to the area being examined, to view the area through a camera lens (with a camera at the tip of the tube), to pump fluids or air in or out, and to pass biopsy or surgical instruments through [3]. When passed through the mouth, an endoscope can be used to examine the esophagus, the stomach, and first part of the small intestine. When passed through the anus, an endoscope can be used to examine the rectum and the entire large intestine.

After the pioneering work of Latham [4], a number of analytical, numerical and experimental studies [5–13] of peristaltic flows of different fluids have been reported under different conditions with reference to physiological and mechanical situations. Several mathematical and experimental models have been developed to understand the chyme movement aspects of peristaltic motion. But less attention has been given to its relevance with endoscope effect. Lew et al. [14] discussed the physiological significance of carrying, mixing, and compression, accompanied by peristalsis. Srivastava [15] devoted his study to observe the effects of an inserted endoscope on chyme movement in small intestine. The important studies of recent years include the investigations of Saxena and Srivastava [16, 17], L.M. Srivastava and V.P. Srivastava [18], Srivastava et al. [19], Cotton and Williams [20], and Abd El-Naby and El-Misery [21].

The aim of present investigation is to investigate the peristaltic motion of chyme, by treating it as Williamson fluid, in the small intestine with an inserted endoscope. For mathematical modeling, we consider the flow in the annular space between two concentric tubes (i.e., outer tube as small intestine and inner tube as endoscope). Moreover, the flow is induced by two sinusoidal peristaltic waves of different wave lengths, traveling along the length of the intestinal wall. The solution of the problem is calculated by two techniques: (i) analytical technique (i.e., regular perturbation method in terms of a variant of Weissenberg number W_e), (ii) numerical technique (i.e., shooting method). The expressions for axial velocity, frictional force, pressure rise, axial pressure gradient and stream function are obtained and the effects of various emerging parameters on the flow characteristics are

illustrated graphically. Streamlines are plotted, and trapping is also discussed. Trapping is an important fluid dynamics phenomenon inherent in peristalsis. At high flow rates and occlusions, there is a region of closed stream lines in the wave frame, and thus, some fluid is found trapped within a wave of propagation. The trapped fluid mass (called bolus) is found to move with the mean speed equal to that of the wave [9].

2. Mathematical Development

We consider the flow of an incompressible, non-Newtonian fluid, bounded between small intestine (outer boundary) and inserted cylindrical endoscope (inner boundary). A physical sketch of the problem is shown in the Figure 1(a). We assume that the peristaltic wave is formed in nonperiodic rush mode composing of two sinusoidal waves of different wave lengths, traveling down the intestinal wall with the same speed c. We consider the cylindrical coordinate system $(\overline{R}, \overline{Z})$ in the fixed frame, where $\overline{Z}$-axis lies along the centerline of the tube, and $\overline{R}$ is transverse to it. Also a symmetry condition is used at the centre.

The geometry of the outer wall surface is described as

$$\overline{h}\left(\overline{Z}, \overline{t}\right) = r_0 + A_1 \sin\frac{2\pi}{\lambda_1}\left(\overline{Z} - c\overline{t}\right) + A_2 \sin\frac{2\pi}{\lambda_2}\left(\overline{Z} - c\overline{t}\right), \tag{2.1}$$

where r_0 is the radius of the outer tube (small intestine), A_1 and λ_1 are the amplitude and the wave length of first wave, A_2 and λ_2 are the amplitude and the wave length of the second wave, c is the propagation velocity, $\overline{t}$ is the time, and $\overline{Z}$ is the axial coordinate.

The governing equations in the fixed frame for an incompressible Williamson fluid model [6] are given as follows:

$$\begin{aligned}
\frac{\partial \overline{U}}{\partial \overline{R}} + \frac{\overline{U}}{\overline{R}} + \frac{\partial \overline{W}}{\partial \overline{Z}} &= 0,\\
\rho\left(\frac{\partial}{\partial \overline{t}} + \overline{U}\frac{\partial}{\partial \overline{R}} + \overline{W}\frac{\partial}{\partial \overline{Z}}\right)\overline{U} &= -\frac{\partial \overline{P}}{\partial \overline{R}} + \frac{1}{\overline{R}}\frac{\partial}{\partial \overline{R}}\left(\overline{R}\overline{\boldsymbol{\tau}}_{\overline{R}\,\overline{R}}\right) + \frac{\partial}{\partial \overline{Z}}\left(\overline{\boldsymbol{\tau}}_{\overline{R}\,\overline{Z}}\right),\\
\rho\left(\frac{\partial}{\partial \overline{t}} + \overline{U}\frac{\partial}{\partial \overline{R}} + \overline{W}\frac{\partial}{\partial \overline{Z}}\right)\overline{W} &= -\frac{\partial \overline{P}}{\partial \overline{Z}} + \frac{1}{\overline{R}}\frac{\partial}{\partial \overline{R}}\left(\overline{R}\overline{\boldsymbol{\tau}}_{\overline{R}\,\overline{Z}}\right) + \frac{\partial}{\partial \overline{Z}}\left(\overline{\boldsymbol{\tau}}_{\overline{Z}\,\overline{Z}}\right),
\end{aligned} \tag{2.2}$$

where $\overline{P}$ is the pressure, and $\overline{U}$,$\overline{W}$ are the respective velocity components in the radial and axial directions in the fixed frame, respectively. Further, the constitutive equation of extra shear stress tensor $\overline{\boldsymbol{\tau}}$ for Williamson fluid [22] is expressed as

$$\overline{\boldsymbol{\tau}} = \left[\mu_\infty + (\mu_0 + \mu_\infty)\left(1 - \Gamma\left|\overline{\dot{\gamma}}\right|\right)^{-1}\right]\overline{\dot{\gamma}}, \tag{2.3}$$

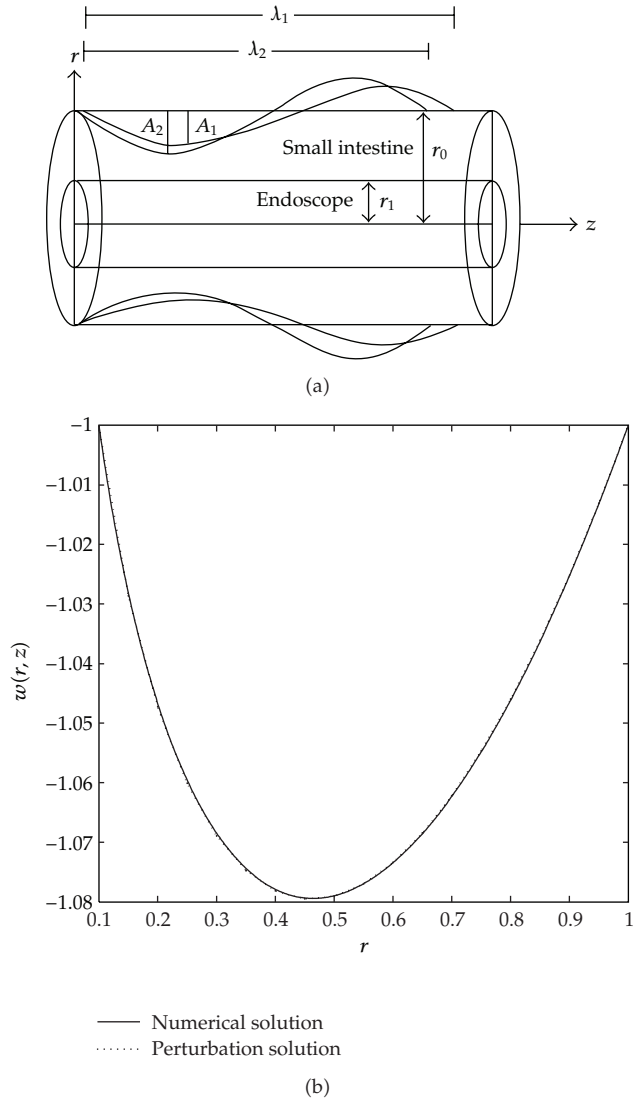

Figure 1: (a) Physical sketch of the problem. (b) Comparison of numerical and perturbation solutions of axial velocity $w(r, z)$ for $W_e = 0.02$, $dp/dz = 0.7$, and $\delta = 0.1$.

where μ_∞ is the infinite shear rate viscosity, μ_0 is the zero shear rate viscosity, Γ is characteristic time and the generalized shear rate $\bar{\dot{\gamma}}$ is expressed in terms of second invariant strain tensor Π as,

$$\left|\bar{\dot{\gamma}}\right| = \sqrt{\frac{1}{2}\sum_i\sum_j \bar{\dot{\gamma}}_{ij}\bar{\dot{\gamma}}_{ji}} = \sqrt{\frac{1}{2}\Pi}, \tag{2.4}$$

in which $\Pi = \mathrm{tr}\,(\mathrm{grad}\mathbf{V} + (\mathrm{grad}\mathbf{V})^T)^2$, and $\mathbf{V}$ denotes the velocity vector.

We consider the case $\mu_\infty = 0$ and $\Gamma|\overline{\dot{\gamma}}| < 1$ for constitutive equation (2.3). Hence, the extra stress tensor can be written as

$$\begin{aligned}\overline{\boldsymbol{\tau}} &= \mu_0\left[\left(1-\Gamma\left|\dot{\gamma}\right|\right)^{-1}\right]\overline{\dot{\gamma}},\\ &= \mu_0\left[\left(1+\Gamma\left|\overline{\dot{\gamma}}\right|\right)\right]\overline{\dot{\gamma}},\end{aligned} \tag{2.5}$$

such that

$$\begin{aligned}\overline{\boldsymbol{\tau}}_{\overline{R}\,\overline{R}} &= 2\mu_0\left(1+\Gamma\left|\overline{\dot{\gamma}}\right|\right)\frac{\partial\overline{U}}{\partial\overline{R}},\\ \overline{\boldsymbol{\tau}}_{\overline{R}\,\overline{Z}} &= \mu_0\left(1+\Gamma\left|\overline{\dot{\gamma}}\right|\right)\left(\frac{\partial\overline{U}}{\partial\overline{Z}}+\frac{\partial\overline{W}}{\partial\overline{R}}\right),\\ \overline{\boldsymbol{\tau}}_{\overline{Z}\,\overline{Z}} &= 2\mu_0\left(1+\Gamma\left|\overline{\dot{\gamma}}\right|\right)\frac{\partial\overline{W}}{\partial\overline{Z}},\\ \left|\overline{\dot{\gamma}}\right| &= \left[2\left(\frac{\partial\overline{U}}{\partial\overline{R}}\right)^2+\left(\frac{\partial\overline{U}}{\partial\overline{Z}}+\frac{\partial\overline{W}}{\partial\overline{R}}\right)^2+2\left(\frac{\partial\overline{W}}{\partial\overline{Z}}\right)^2\right]^{1/2}.\end{aligned} \tag{2.6}$$

In the fixed coordinates $(\overline{R},\overline{Z})$, the flow is unsteady. It becomes steady in a wave frame $(\overline{r},\overline{z})$ moving with the same speed as the wave moves in the $\overline{Z}$-direction. The transformations between the two frames are

$$\begin{aligned}\overline{r} &= \overline{R}, \qquad \overline{z} = \overline{Z} - c\overline{t},\\ \overline{u} &= \overline{U}, \qquad \overline{w} = \overline{W} - c,\end{aligned} \tag{2.7}$$

in which $\overline{u}$ and $\overline{w}$ are the velocities in the wave frame. The corresponding boundary conditions in the wave frame are

$$\begin{aligned}\overline{w} &= -c, \quad \text{at } \overline{r} = \overline{r}_1,\\ \overline{w} &= -c, \quad \text{at } \overline{r} = \overline{h} = r_0 + A_1\sin\frac{2\pi}{\lambda_1}(\overline{z}) + A_2\sin\frac{2\pi}{\lambda_2}(\overline{z}),\end{aligned} \tag{2.8}$$

where $\overline{r}_1$ is the radius of the inner tube (endoscope). In order to reduce the number of variables, we introduce the following nondimensional variables:

$$\begin{gathered}R = \frac{\overline{R}}{r_0}, \qquad r = \frac{\overline{r}}{r_0}, \qquad Z = \frac{\overline{Z}}{\lambda_1}, \qquad z = \frac{\overline{z}}{\lambda_1}, \qquad W = \frac{\overline{W}}{c}, \qquad w = \frac{\overline{w}}{c}, \qquad \boldsymbol{\tau} = \frac{r_0\overline{\boldsymbol{\tau}}}{c\mu_0},\\ U = \frac{\lambda_1\overline{U}}{r_0c}, \qquad u = \frac{\lambda_1\overline{u}}{r_0c}, \qquad p = \frac{r_0\overline{P}}{c\lambda_1\mu_0}, \qquad t = \frac{c\overline{t}}{\lambda_1}, \qquad R_e = \frac{\rho c r_0}{\mu_0}, \qquad W_e = \frac{\Gamma c}{r_0},\\ h = \frac{\overline{h}}{r_0} = 1 + \phi_1\sin 2\pi z + \phi_2\sin 2\pi\gamma z, \qquad r_1 = \frac{\overline{r}_1}{r_0}, \qquad \delta = \frac{r_1}{r_0}, \qquad \phi_1 = \frac{A_1}{r_0},\\ \phi_2 = \frac{A_2}{r_0}, \qquad \gamma = \frac{\lambda_1}{\lambda_2}, \qquad \epsilon = \frac{r_0}{\lambda_1}.\end{gathered} \tag{2.9}$$

Here R_e, W_e, and ϵ represent the Reynolds number, Weissenberg number, and wave number, respectively. Moreover, ϕ_1 and ϕ_2 are nondimensional amplitudes of the waves, δ is the annulus aspect ratio, and γ represents the wave length ratio between two waves. By using (2.7) and (2.9), we get

$$\begin{aligned}
\frac{\partial u}{\partial r}+\frac{u}{r}+\frac{\partial w}{\partial z}&=0,\\
R_e\epsilon^3\left(u\frac{\partial}{\partial r}+w\frac{\partial}{\partial z}\right)u&=-\frac{\partial p}{\partial r}+\frac{\epsilon}{r}\frac{\partial}{\partial r}(r\boldsymbol{\tau}_{rr})+\epsilon^2\frac{\partial}{\partial z}(\boldsymbol{\tau}_{rz}),\\
R_e\epsilon\left(u\frac{\partial}{\partial r}+w\frac{\partial}{\partial z}\right)w&=-\frac{\partial p}{\partial z}+\frac{1}{r}\frac{\partial}{\partial r}(r\boldsymbol{\tau}_{rz})+\epsilon\frac{\partial}{\partial z}(r\boldsymbol{\tau}_{zz}),
\end{aligned}\tag{2.10}$$

and components of the extra stress tensor take the following form:

$$\begin{aligned}
\boldsymbol{\tau}_{rr}&=2\epsilon\left[1+W_e|\dot{\gamma}|\right]\frac{\partial u}{\partial r},\\
\boldsymbol{\tau}_{rz}&=\left[1+W_e|\dot{\gamma}|\right]\left(\frac{\partial u}{\partial z}\epsilon^2+\frac{\partial w}{\partial r}\right),\\
\boldsymbol{\tau}_{zz}&=2\epsilon\left[1+W_e|\dot{\gamma}|\right]\frac{\partial w}{\partial z},\\
|\dot{\gamma}|&=\left[2\epsilon^2\left(\frac{\partial u}{\partial r}\right)^2+\left(\frac{\partial w}{\partial r}+\frac{\partial u}{\partial z}\epsilon^2\right)^2+2\epsilon^2\left(\frac{\partial w}{\partial r}\right)^2\right]^{1/2}.
\end{aligned}\tag{2.11}$$

Under the assumption of long wavelength $\epsilon \ll 1$ and low Reynolds number approximations, the above equations are further reduced to

$$\frac{\partial p}{\partial r}=0,\tag{2.12}$$

$$-\frac{\partial p}{\partial z}+\frac{1}{r}\frac{\partial}{\partial r}(r\boldsymbol{\tau}_{rz})=0,\tag{2.13}$$

$$\boldsymbol{\tau}_{rz}=\frac{\partial w}{\partial r}+W_e\left(\frac{\partial w}{\partial r}\right)^2.\tag{2.14}$$

Equation (2.12) shows that $p=p(z)$. Now putting expression of $\boldsymbol{\tau}_{rz}$ in (2.13) we get

$$-\frac{\partial p}{\partial z}+\frac{1}{r}\left[r\left(\frac{\partial w}{\partial r}+W_e\left(\frac{\partial w}{\partial r}\right)^2\right)\right]=0.\tag{2.15}$$

The corresponding nondimensional boundary conditions thus obtained are

$$\begin{aligned}
w&=-1\quad \text{at } r=\delta,\\
w&=-1\quad \text{at } r=h=h(z)=1+\phi_1\sin 2\pi z+\phi_2\sin 2\pi\gamma z.
\end{aligned}\tag{2.16}$$

3. Solution of the Problem

3.1. Perturbation Solution

Since (2.15) is a nonlinear equation and the exact solution may not be possible, therefore, in order to find the solution, we employ the regular perturbation method in terms of a variant of Weissenberg number W_e. For perturbation solution, we expand w and p as

$$\begin{aligned} w &= w_0 + W_e w_1 + O\left(W_e^2\right), \\ p &= p_0 + W_e p_1 + O\left(W_e^2\right). \end{aligned} \tag{3.1}$$

To first order, the expressions for axial velocity and axial pressure gradient satisfying boundary conditions (2.16) directly yield

$$w(r,z) = -1 + 0.25\frac{dp}{dz}(a_{45}) + W_e\frac{dp}{dz}(a_{46} - a_{47}), \tag{3.2}$$

$$\frac{dp}{dz} = a_{48}(a_{49} + a_{50} - a_{51} + a_{52}), \tag{3.3}$$

where the involved quantities are defined in Appendix.

The expressions of pressure rise Δp and the frictional forces F_0 and F_1 at the outer and inner boundaries, respectively, in their nondimensional forms, are given as

$$\Delta p = \int_0^1 \frac{dp}{dz}dz, \tag{3.4}$$

$$F_0 = \int_0^1 \delta^2\left(-\frac{dp}{dz}\right)dz, \tag{3.5}$$

$$F_1 = \int_0^1 h^2\left(-\frac{dp}{dz}\right)dz. \tag{3.6}$$

where dp/dz is defined through (3.3), and flow rate Q in dimensionless form is defined as

$$Q = q - \pi\left(\left\langle h^2\right\rangle - \delta^2\right), \tag{3.7}$$

where q is flow rate in the fixed frame of reference, and $\langle h^2\rangle$ is square of displacement of the walls over the length of an annulus, defined as

$$\left\langle h^2\right\rangle = \int_0^1 \left(h^2\right)dz. \tag{3.8}$$

Table 1: Numerical and perturbation solutions for axial velocity $w(r,z)$.

r	Numerical Sol. $w(r,z)$	Perturbation Sol. $w(r,z)$	Error
0.10	−1.0000	−1.0000	0.0000
0.15	−1.0284	−1.0286	0.0002
0.20	−1.0470	−1.0473	0.0003
0.25	−1.0599	−1.0601	0.0002
0.30	−1.0687	−1.0689	0.0002
0.35	−1.0745	−1.0748	0.0003
0.40	−1.078	−1.0781	0.0001
0.45	−1.0794	−1.0795	0.0001
0.50	−1.0790	−1.0790	0.0000
0.55	−1.0770	−1.0770	0.0000
0.60	−1.0734	−1.0734	0.0000
0.65	−1.0685	−1.0684	0.0001
0.70	−1.0622	−1.0622	0.0000
0.75	−1.0546	−1.0547	0.0001
0.80	−1.0461	−1.0460	0.0001
0.85	−1.0362	−1.0361	0.0001
0.90	−1.0251	−1.0252	0.0001
0.95	−1.0128	−1.0131	0.0003
1.0	−1.0000	−1.0000	0.0000

Also in order to establish stream lines, we obtain stream function by using the following relation:

$$u = -\frac{1}{r}\frac{\partial \psi}{\partial z}, \qquad w = \frac{1}{r}\frac{\partial \psi}{\partial r}, \tag{3.9}$$

which yields

$$\psi = \frac{r}{480}(a_{30}) + a_{31}\Big[\Big(a_{32} - a_{33} - a_{34} + 5a_{26}a_{12}^2 - a_{35}\Big) \times a_{36} - a_{37} - a_{38} + a_{39} + \ a_{40} + a_{41} - a_{42} + a_{43} + a_{44}\Big], \tag{3.10}$$

where the involved quantities are defined in Appendix.

3.2. Numerical Solution

Equation (2.15) is solved numerically by using shooting method [23]. The numerical result for axial velocity $w(r,z)$ is compared with the perturbation result, and both results reveal a very good agreement with each other, as demonstrated in Table 1 and Figure 1(b).

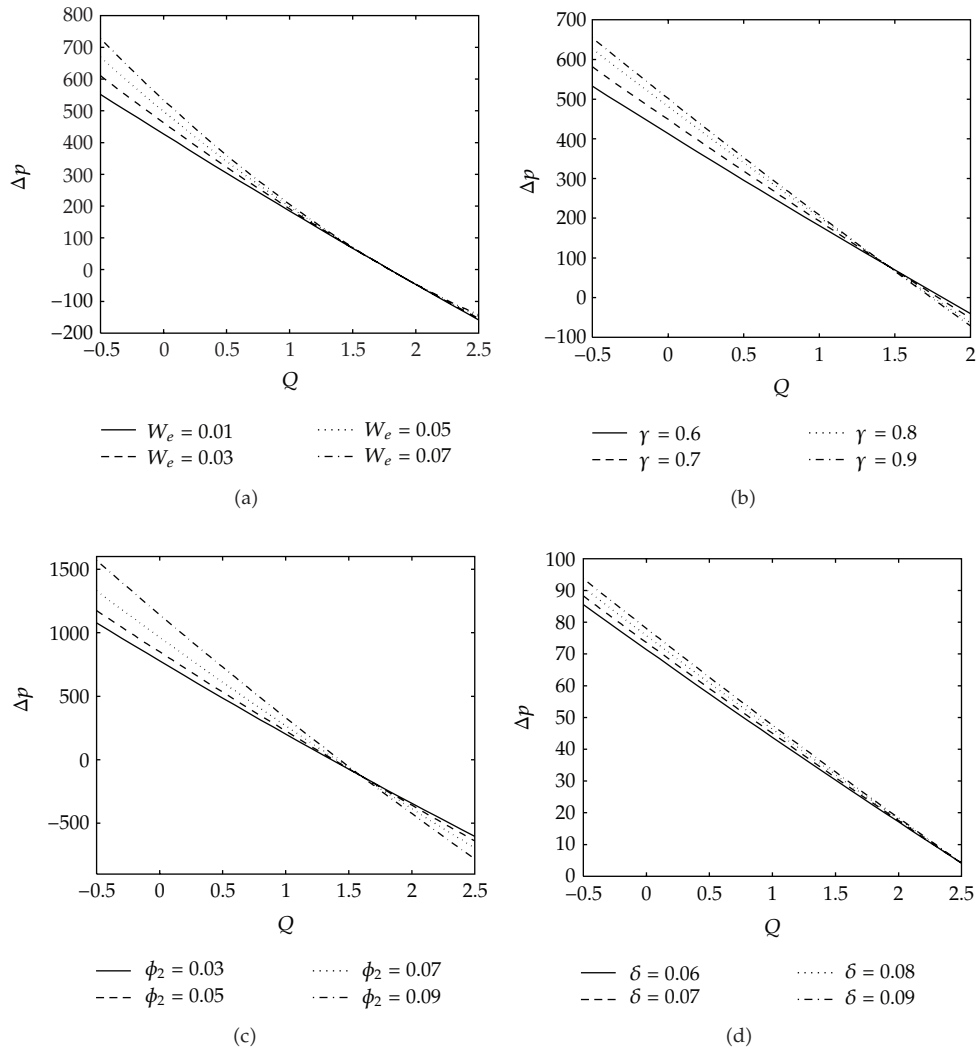

Figure 2: Variation of pressure rise per wavelength (Δp) for different values of (a) W_e with $\phi_1 = 0.03$, $\phi_2 = 0.05$, $Q = 0.2$, $\delta = 0.7$ and $\gamma = 0.9$, (b) γ with $\phi_1 = 0.03$, $\phi_2 = 0.05$, $Q = 2$, $\delta = 0.7$, and $W_e = 0.01$, (c) ϕ_2 with $\phi_1 = 0.01$, $Q = 0.2$, $\gamma = 0.9$, $\delta = 0.7$, and $W_e = 0.01$, and (d) δ with $\phi_1 = 0.03$, $\phi_2 = 0.05$, $Q = 0.2$, $\gamma = 0.9$, and $W_e = 0.01$.

4. Graphical Results and Discussion

In this section, the graphical representations of the obtained solutions are demonstrated along with their respective explanation. The expressions for pressure rise and frictional forces are not found analytically; therefore, MATHEMATICA software is used to perform the integration in order to analyze their graphical behavior. It is also pertinent to mention that the values of all embedded flow parameters are considered to be less than 1.

Figures 2(a) to 2(d) are graphs of pressure rise Δp versus flow rate Q to show the effects of different parameters on pumping rate. For peristaltic pumping, we divide the whole

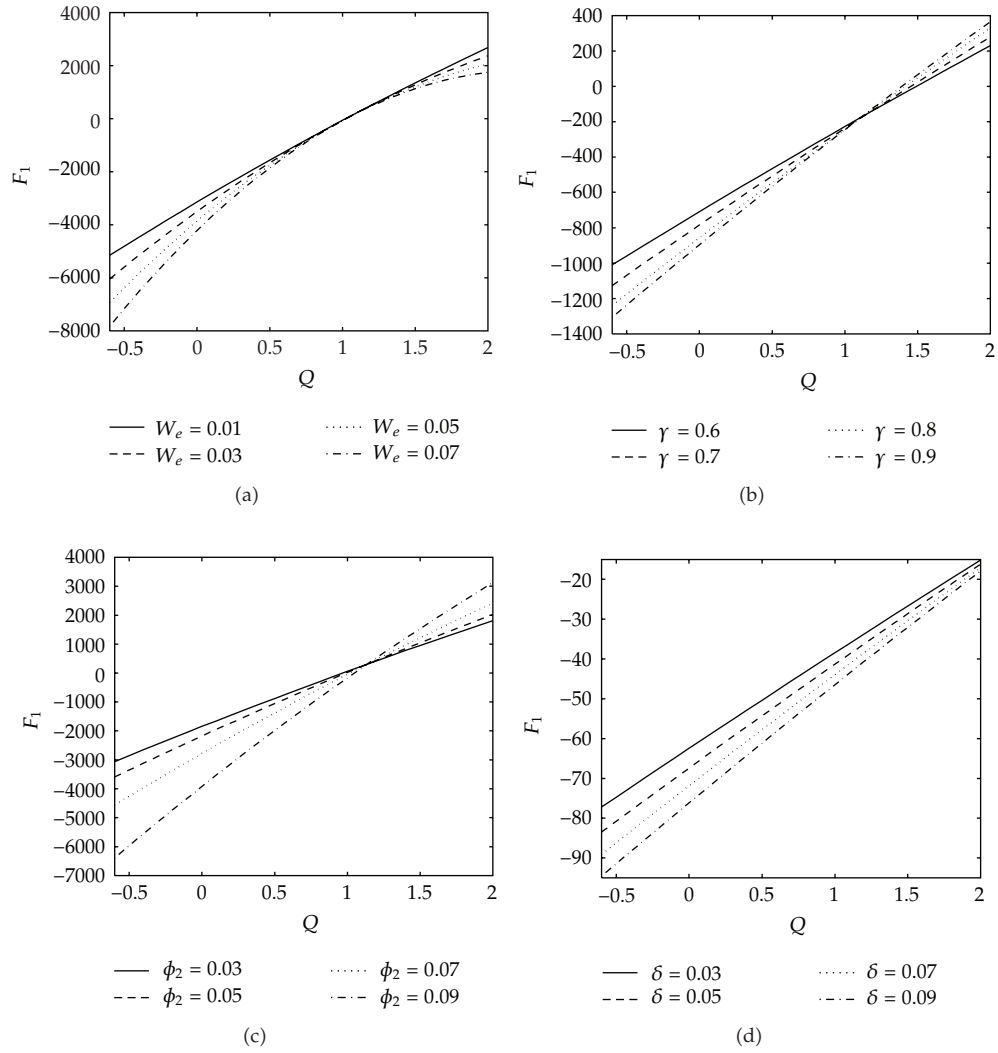

Figure 3: Variation of frictional force at the inner wall (F_1) for different values of (a) W_e with $\phi_1 = 0.03$, $\phi_2 = 0.05$, $Q = 2$, $\delta = 0.7$, and $\gamma = 0.9$, (b) γ with $\phi_1 = 0.03$, $\phi_2 = 0.05$, $Q = 0.2$, $\delta = 0.7$, and $W_e = 0.01$, (c) ϕ_2 with $\phi_1 = 0.01$, $Q = 0.2$, $\gamma = 0.9$, $\delta = 0.7$ and $W_e = 0.01$, and (d) δ with $\phi_1 = 0.03$, $\phi_2 = 0.05$, $Q = 0.2$, $\gamma = 0.9$ and $W_e = 0.01$.

region into three parts. The region corresponding to $\Delta p > 0$ and $Q > 0$ is known as the peristaltic pumping region. At $\Delta p = 0$ is the free pumping region. And the region at $\Delta p < 0$ and $Q > 0$ is called augmented pumping. Figure 2(a) shows that the pumping rate decreases by increasing the values of Weissenberg number W_e, and this behavior remains the same in all three pumping regions. Figure 2(b) indicates the effect of the wavelength ratio γ on Δp. Here, pressure rise decreases with an increase in γ peristaltic pumping region, and after a critical value of $Q = 1.4$, it increases in the free and augmented pumping regions. Figure 2(c) explains the effect of the amplitude ratio ϕ_2 on Δp. Here, pressure rise decreases with an

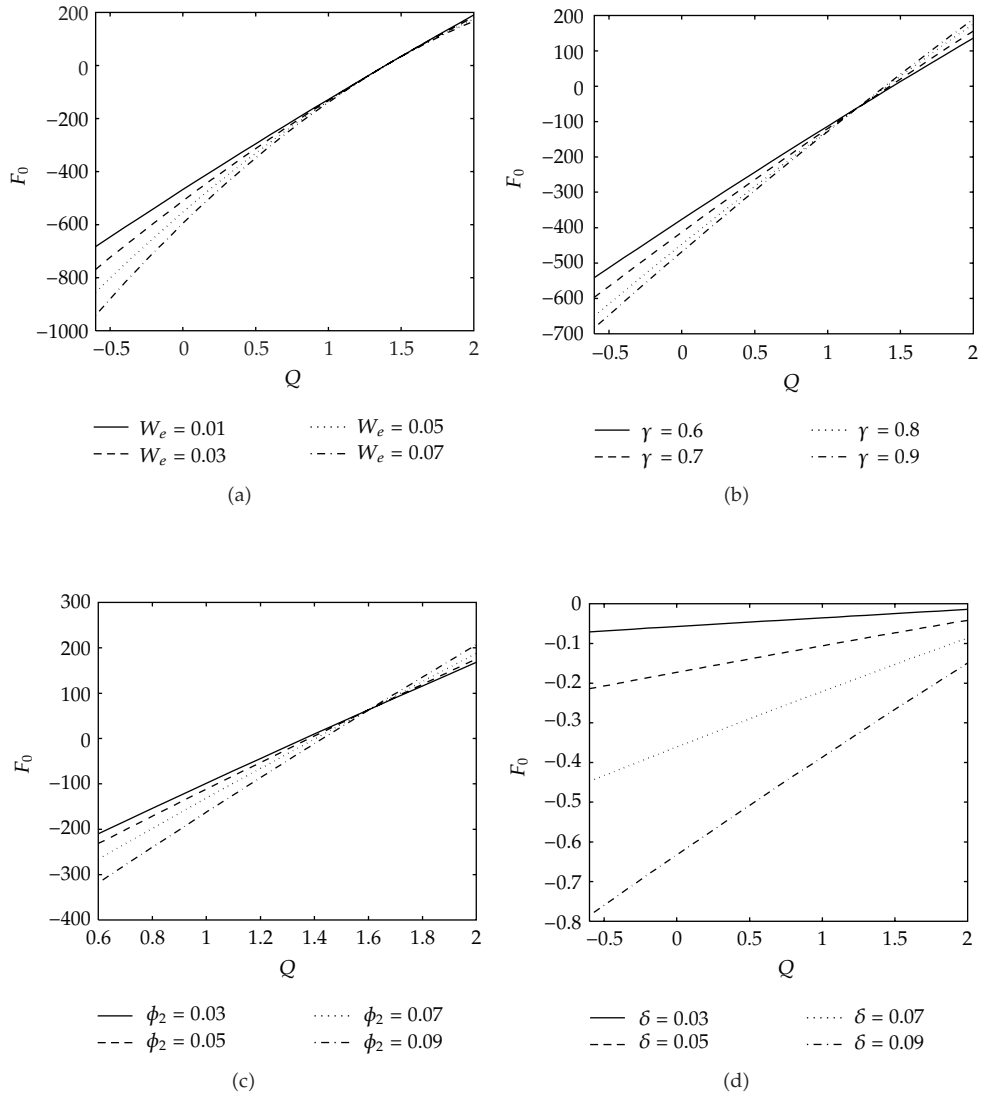

Figure 4: Variation of frictional force at the outer wall (F_0) for different values of (a) W_e with $\phi_1 = 0.03$, $\phi_2 = 0.05$, $Q = 0.2$, $\delta = 0.7$, and $\gamma = 0.9$, (b) γ with $\phi_1 = 0.03$, $\phi_2 = 0.05$, $Q = 2$, $\delta = 0.7$, and $W_e = 0.01$, (c) ϕ_2 with $\phi_1 = 0.01$,$Q = 0.2$, $\gamma = 0.9$, $\delta = 0.7$, and $W_e = 0.01$, and (d) δ with $\phi_1 = 0.03$, $\phi_2 = 0.05$, $Q = 0.2$, $\gamma = 0.9$ and $W_e = 0.01$.

increase in value of ϕ_2 in the free and peristaltic pumping region, and after a critical value of $Q = 1.5$, it increases in the augmented pumping region. Figure 2(d) shows that pressure rise decreases when annulus aspect ratio δ increases.

Similarly the effects of W_e, γ, ϕ_2, and δ on frictional forces are plotted in Figures 3-4. Figures 3(a) to 3(d) represent the variation of the frictional force at the outer wall (F_0) and Figures 4(a) to 4(d) indicate the variation of the frictional force at the inner wall (F_1) with

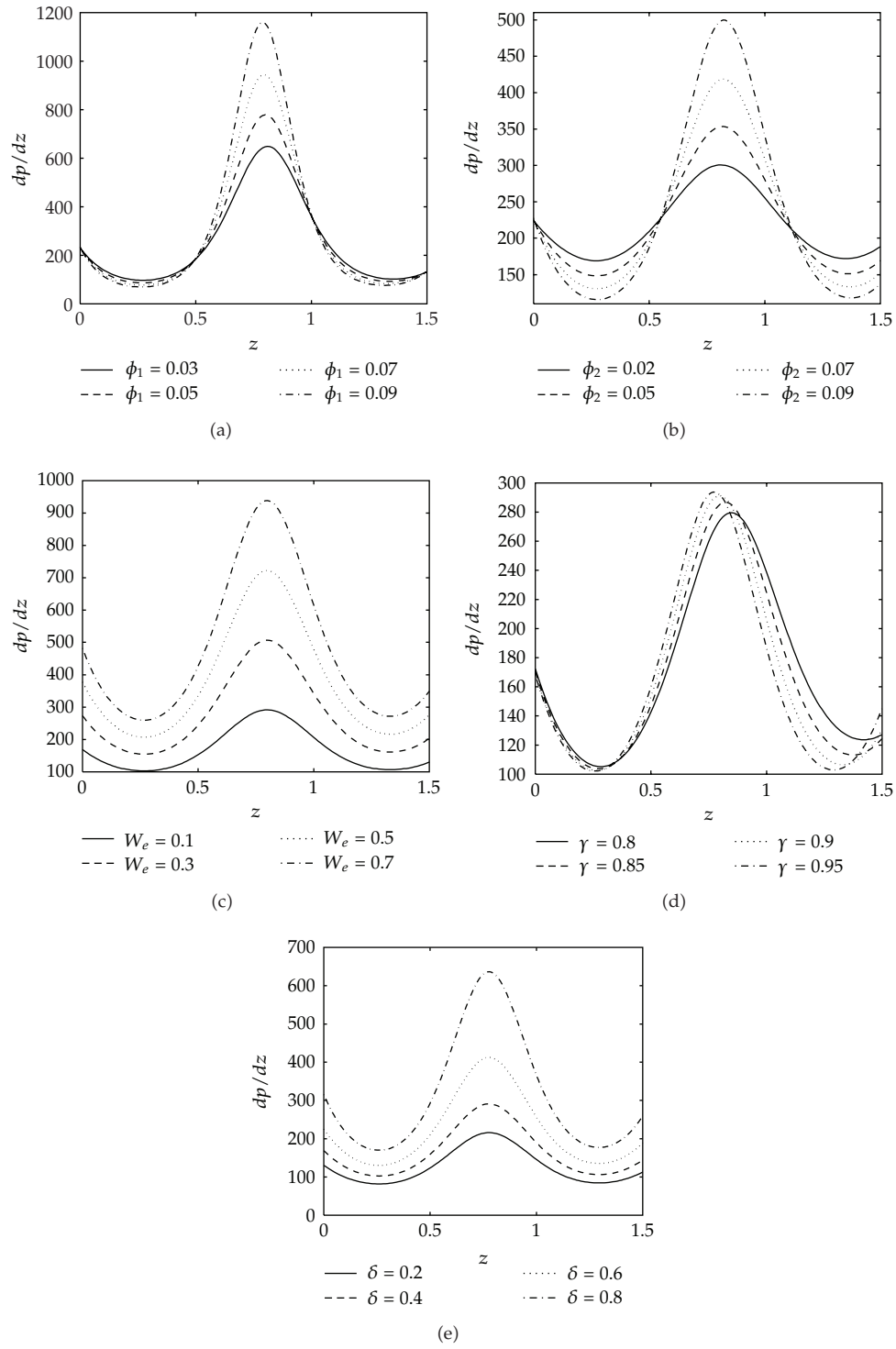

Figure 5: Pressure gradient dP/dz verses z for different values of (a) ϕ_1 with $\phi_2 = 0.06$, $Q = 0.2$, $\gamma = 0.9$, $\delta = 0.5$, and $W_e = 0.05$, (b) ϕ_2 with $\phi_1 = 0.06$, $Q = 0.2$, $\gamma = 0.9$, $\delta = 0.5$, and $W_e = 0.05$, (c) W_e. with $\phi_1 = 0.04$, $\phi_2 = 0.06$, $Q = 0.2$, $\delta = 0.5$, and $\gamma = 0.9$, (d) δ with $\phi_1 = 0.04$, $\phi_2 = 0.06$, $Q = 0.2$, $\gamma = 0.9$ and $W_e = 0.05$, and (e) γ with $\phi_1 = 0.04$, $\phi_2 = 0.06$, $Q = 0.2$, $\delta = 0.5$ and $W_e = 0.05$.

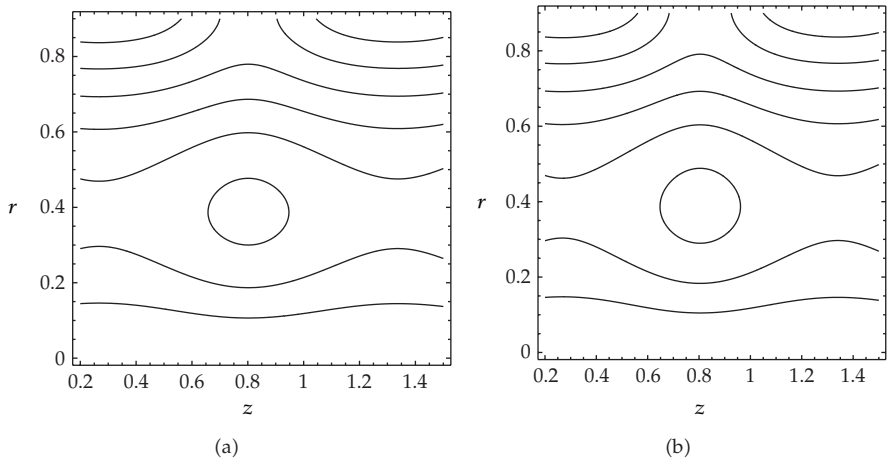

Figure 6: Streamlines pattern for (a) $\phi_2 = 0.08$ (b) $\phi_2 = 0.09$ with $\phi_1 = 0.04$, $Q = 0.2$, $\delta = 0.4$, $\gamma = 0.9$ and $W_e = 0.03$.

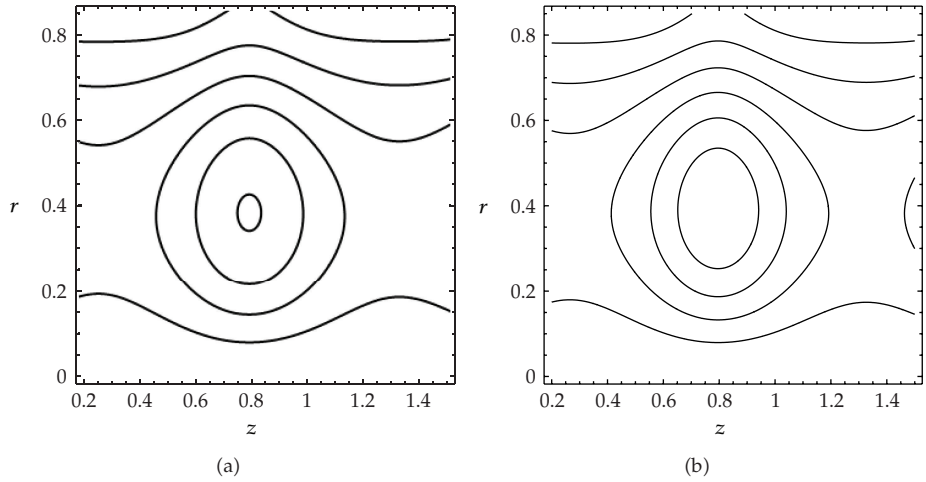

Figure 7: Streamlines pattern for (a) $W_e = 0.01$ (b) $W_e = 0.02$ with $\phi_1 = 0.04$, $\phi_2 = 0.06$, $Q = 0.2$, $\gamma = 0.9$ and $\delta = 0.4$.

flow rate Q. It can be noted that the phenomena presented in these figures possess opposite character to the pressure rise for any given set of parameters. Also the graphs of both F_0 and F_1 show similar behavior when compared to their respective parameters. It is significant to mention that inner friction force F_1 attains higher magnitude than outer friction force F_0 with increasing values of any given set of parameters.

In order to discuss the effects of variation of various parameters on the axial pressure gradient dp/dz, MATHEMATICA has been used for the numerical evaluation of the analytical results, and the results are graphically presented in Figures 5(a) to (5(e). In these figures, the pressure gradient distribution for various values of ϕ_1, ϕ_2, W_e, γ, and δ is depicted. It is observed that pressure gradient increases with increasing the values of previously mentioned parameters.

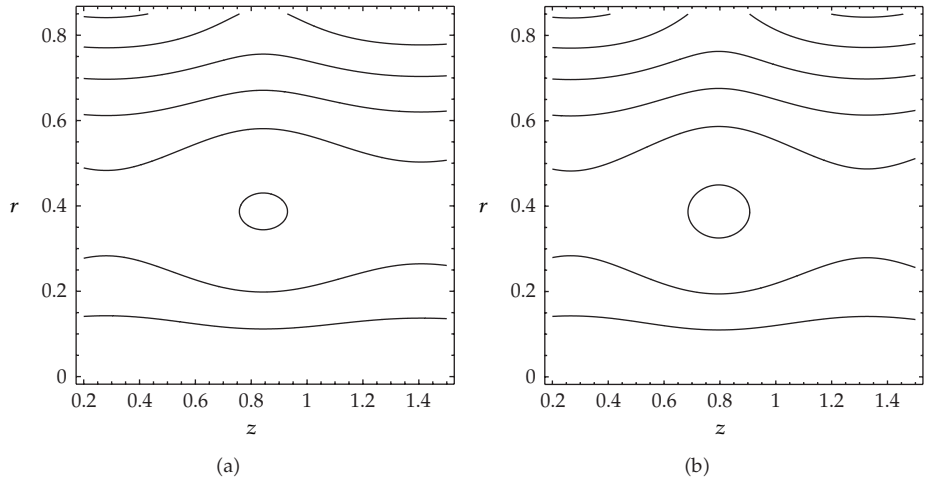

Figure 8: Streamlines pattern for (a) $\gamma = 0.8$ (b) $\gamma = 0.9$ with $\phi_1 = 0.04$, $\phi_2 = 0.06$, $Q = 0.2$, $\delta = 0.4$ and $W_e = 0.03$.

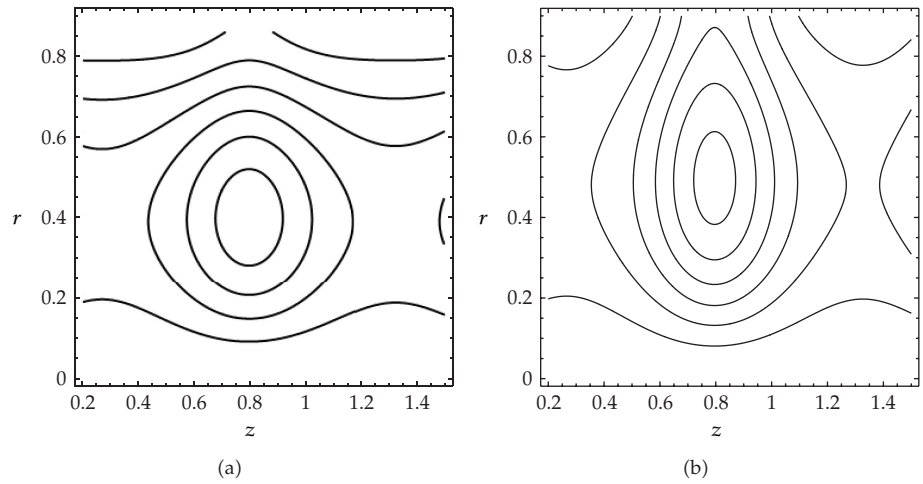

Figure 9: Streamlines pattern for (a) $\delta = 0.4$ (b) $\delta = 0.5$ with $\phi_1 = 0.04$, $\phi_2 = 0.06$, $Q = 0.2$, $\gamma = 0.9$ and $W_e = 0.03$.

The influence of various parameters on streamlines pattern is depicted in Figures 6, 7, 8, 9, and 10. It is noted that trapping is observed in all these cases. Figures 6, 7, 8, and 9 show that the size of trapped bolus increases for higher values of Weissenberg number (W_e), wave length ratio (γ), and amplitude (ϕ_2). Figure 9 exhibits the effects of radius ratio (δ) on streamlines pattern. It can be seen that the size and number of the trapped bolus increase with an increase in δ. However, the size and number of trapped bolus decrease with increasing values of flow rate as shown in Figure 10.

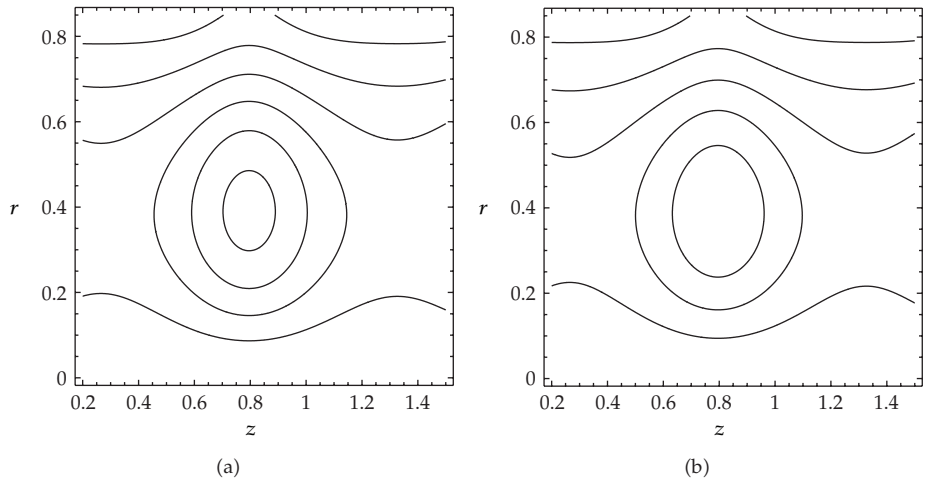

Figure 10: Streamlines pattern for (a) $Q = 0.3$ (b) $Q = 0.5$ with $\phi_1 = 0.04$, $\phi_2 = 0.06$, $\gamma = 0.9$, $\delta = 0.4$ and $W_e = 0.03$.

5. Conclusion

The peristaltic flow of chyme (treated as Williamson fluid) in small intestine with an inserted endoscope is investigated. The flow is considered between annular space of small intestine and inserted endoscope and is induced by two sinusoidal peristaltic waves of different wave lengths, traveling along the length of the intestinal wall. Long wavelength and low Reynolds number approximations are used to simplify the resulting equations. The solution of the problem is calculated using analytical technique (i.e., regular perturbation method) and numerical technique (i.e., shooting method). Also results of axial velocity for both solutions are compared and found a very good agreement between them.

The performed analysis can be concluded as follows:

(1) the peristaltic pumping rate decreases with increasing the values of ϕ_2, W_e, γ, and δ. This shows that the effects of these parameters on the pressure rise are qualitatively similar;

(2) frictional forces show an opposite behavior to that of pressure rise in peristaltic transport;

(3) the inner friction force F_1 attains higher magnitude than outer friction force F_0 with increasing values of any given set of parameters;

(4) Pressure gradient increases with increasing the values of all embedded parameters that is, ϕ_1, ϕ_2, W_e, γ, and δ;

(5) an increase in radius ratio (δ) results in the increase of the size and number of trapped bolus. Also the size of trapped bolus increases for higher values of amplitude rate (ϕ_2), Weissenberg number (W_e), and wave length ratio (γ);

(6) moreover, it is observed that the size and number of trapping bolus decrease with increasing values of flow rate (Q).

Appendix

The values of quantities appearing in the expressions (3.2), (3.3), and (3.4) are given as

$$a_{11} = \log h + \log r, \quad a_{12} = \log h + \log \delta, \quad a_{13} = h^2 - r^2,$$
$$a_{14} = h^2 - \delta^2, \quad a_{15} = h - r, \quad a_{16} = h - \delta, \quad a_{17} = h + \delta,$$
$$a_{18} = h^2 + \delta^2, \quad a_{19} = h^2 + r^2, \quad a_{20} = h^4 - \delta^4, \quad a_{21} = h^6 - \delta^6,$$
$$a_{22} = h^3 + \delta^3, \quad a_{23} = h^5 - \delta^5, \quad a_{24} = h^2 + \delta^2, \quad a_{25} = h^3 - \delta^3,$$
$$a_{26} = h^7 - \delta^7, \quad a_{27} = h^4 + \delta^4, \quad a_{28} = \log \delta^3 - \log h^3,$$
$$a_{29} = \log h \log \delta, \quad a_{30} = \frac{240 r a_{28} + 720 r a_{29} a_{12}}{a_{12}^3},$$
$$a_{31} = \frac{r(2Q + a_{14})}{\left(300 h \delta a_{16}^2 a \log \delta_{17}^3 (-a_{14} + a_{24} a_{12})\right)^3},$$
$$a_{32} = -10 W_e a_{16}^3 a_{17}^3 a_{12} (2Q + a_{14}),$$
$$a_{33} = h \delta a_{12} \left(5 a_{16}^2 a_{17}^2\right) (-24 Q W_e + a_{14} a_{12} (-12 W_e + a_{17})),$$
$$a_{34} = 10 a_{14} a_{12} (a_{23} - 8 Q W_e (a_{24} + h\delta) - 4 h \delta (W_e (a_{14} + a_{20}) + a_{25})),$$
$$a_{35} = 32 Q a_{12}^2 W_e \left(a_{27} + h \delta a_{14} + h^2 \delta^2\right) + 16 W_e (a_{21} - h \delta a_{27} + 5 h \delta a_{23}) a_{12}^3,$$
$$a_{36} = 30 r^3 - 8 r^4 W_e - \frac{15 r W_e a_{16}^3 a_{17}}{\delta a_{12}^3} \left(\frac{a_{17}}{h} + \log h\right),$$
$$a_{37} = \frac{1}{a_{12}^3} 10 r \left(h^3 W_e + \delta^2 (3 - 7 W_e \delta) + h^2 (-3 + 6 W_e \delta) \log h^2\right),$$
$$a_{38} = 20 r \delta^2 (3 - W_e \delta) \log h^3 + 5 a_{16} r \log r \left(3 a_{12} \frac{a_{16}^2 a_{17}^2}{h\delta} - 12 a_{14} a_{12}^2\right),$$
$$a_{39} = 4 W_e^2 a_{12} (a_{24} + h\delta - a_{17}),$$
$$a_{40} = \frac{r a_{16}}{a_{12}^3} \left(\frac{15 W_e}{h} a_{14} \log \delta + 80 h^2 W_e + 20 \delta (-3 + 4 W_e \delta)\right),$$
$$a_{41} = 20 h (-3 + 7 W_e \delta) a_{29} + a_{29} \log h \left(60 h - 20 h^3 W_e + 120 \delta^2 - 40 \delta^3 W_e\right),$$
$$a_{42} = 70 h^2 W_e + 10 \delta (-3 + W_e \delta) + 10 h (-3 + 7 W_e \delta) \log \delta^2,$$
$$a_{43} = \frac{r a_{29} \log \delta}{a_{12}^3} \left(-120 h^2 + 40 h^3 W_e - 60 \delta^2 + 20 \delta^3 W_e\right),$$
$$a_{44} = \frac{20 r h^2 \log \delta^3}{a_{12}^3} (3 - h W_e), \quad a_{45} = -a_{13} + \frac{a_{11} a_{16}}{a_{12}} a_{17},$$
$$a_{46} = \frac{a_{15}}{12} (a_{19} + hr) + \frac{a_{15}^2 a_{16} a_{17}^2}{16 a_{12}^2} + \frac{a_{16}^2 a_{17}^2 a_{11}}{16 a_{12}^2},$$

$$
\begin{aligned}
a_{47} &= \frac{a_{15}a_{14}}{4a_{12}} + \frac{a_{11}a_{16}}{12a_{12}}(a_{18}+h\delta) + \frac{a_{16}^3 a_{17}^2 a_{11}}{16h\delta(a_{12})^3},\\
a_{48} &= \frac{1}{5h\delta a_{16}^2 a_{17}^3(-a_{14}+a_{18}a_{12})^3},\\
a_{49} &= 8\Big((2Q+a_{14})\Big(-5h\delta a_{16}^3 a_{17}a_{12}\Big) + 10h\delta a_{14}(a_{23}-h\delta a_{22})a_{12}^2 + a_{12}^2\Big),\\
a_{50} &= 8W_e\Big(-10a_{16}^3 a_{17}^3(2Q+a_{14})^2 + 60h\delta a_{16}^2 a_{17}^2 a_{12}(2Q+a_{14})\Big),\\
a_{51} &= 40h\delta a_{14}a_{12}^2(2Qa_{18}+a_{20}+a_{14})(2Qa_{18}+a_{20}+a_{14}),\\
a_{52} &= 16h\delta a_{12}^3 2Q\Big(a_{20}+h^2\delta a_{17}+h\delta^3\Big) + a_{21} + h\delta a_{20}.
\end{aligned}
\tag{A.1}
$$

Acknowledgments

The first and second author is thankful to higher education of Pakistan for the financial support and the third author extends his appreciation to the deanship of Scientific Research at king Saud University for funding this work through the research group Project no. RGP-VPP-080.

References

[1] L. M. Srivastava and V. P. Srivastava, "Peristaltic transport of a non-Newtonian fluid: applications to the vas deferens and small intestine," *Annals of Biomedical Engineering*, vol. 13, no. 2, pp. 137–153, 1985.

[2] S. Keshav, *The Gastrointestinal System at a Glance*, Wiley-Blackwell, Malden, Mass, USA, 2003.

[3] H. G. Beger, A. Schwarz, and U. Bergmann, "Progress in gastrointestinal tract surgery: the impact of gastrointestinal endoscopy," *Surgical Endoscopy and Other Interventional Techniques*, vol. 17, no. 2, pp. 342–350, 2003.

[4] T. W. Latham, *Fluid Motion in a Peristaltic Pump*, M.S. thesis, Massachusetts Institute of Technology, Cambridge, Mass, USA, 1966.

[5] S. Srinivas and R. Gayathri, "Peristaltic transport of a Newtonian fluid in a vertical asymmetric channel with heat transfer and porous medium," *Applied Mathematics and Computation*, vol. 215, no. 1, pp. 185–196, 2009.

[6] S. Srinivas, R. Gayathri, and M. Kothandapani, "The influence of slip conditions, wall properties and heat transfer on MHD peristaltic transport," *Computer Physics Communications*, vol. 180, no. 11, pp. 2115–2122, 2009.

[7] M. Kothandapani and S. Srinivas, "Peristaltic transport of a Jeffrey fluid under the effect of magnetic field in an asymmetric channel," *International Journal of Non-Linear Mechanics*, vol. 43, no. 9, pp. 915–924, 2008.

[8] S. Srinivas and M. Kothandapani, "Peristaltic transport in an asymmetric channel with heat transfer. A note," *International Communications in Heat and Mass Transfer*, vol. 35, no. 4, pp. 514–522, 2008.

[9] A. H. Sharpio, M. Y. Jaffrin, B. R. P. Rao, and S. I. Weinberg, "Peristaltic pumping with long wavelength and low Reynolds number," *Journal of Fluid Mechanics*, vol. 37, no. 4, pp. 799–825, 1969.

[10] S. Nadeem and N. S. Akbar, "Numerical solutions of peristaltic flow of Williamson fluid with radially varying MHD in an endoscope," *International Journal for Numerical Methods in Fluids*, vol. 66, no. 2, pp. 212–220, 2011.

[11] S. Nadeem, N. S. Akbar, and M. Y. Malik, "Numerical solutions of peristaltic flow of a Newtonian fluid under the effects of magnetic field and heat transfer in a porous concentric tubes," *Zeitschrift fur Naturforschung A*, vol. 65, no. 5, pp. 369–389, 2010.

[12] S. Nadeem and N. S. Akbar, "Effects of heat transfer on the peristaltic transport of MHD Newtonian fluid with variable viscosity: application of a domain decomposition method," *Communications in Nonlinear Science and Numerical Simulation*, vol. 14, pp. 3844–3855, 2009.

[13] S. Nadeem, T. Hayat, N. S. Akbar, and M. Y. Malik, "On the influence of heat transfer in peristalsis with variable viscosity," *International Journal of Heat and Mass Transfer*, vol. 52, no. 21-22, pp. 4722–4730, 2009.

[14] H. S. Lew, Y. C. Fung, and C. B. Lowenstein, "Peristaltic carrying and mixing of chyme in the small intestine," *Journal of Biomechanics*, vol. 4, no. 4, pp. 297–315, 1971.

[15] V. P. Srivastava, "Effects of an inserted endoscope on chyme movement in small intestine—a theoretical model," *Applications and Applied Mathematics*, vol. 2, no. 2, pp. 79–91, 2007.

[16] M. Saxena and V. P. Srivastava, "Particulate suspension flow induced by sinusoidal peristaltic waves," *Japanese Journal of Applied Physics*, vol. 36, no. 1 A, pp. 385–390, 1997.

[17] V. P. Srivastava and M. Saxena, "A two-fluid model of non-Newtonian blood flow induced by peristaltic waves," *Rheologica Acta*, vol. 34, no. 4, pp. 406–414, 1995.

[18] L. M. Srivastava and V. P. Srivastava, "Peristaltic transport of blood: casson model. II," *Journal of Biomechanics*, vol. 17, no. 11, pp. 821–829, 1984.

[19] L. M. Srivastava, V. P. Srivastava, and S. N. Sinha, "Peristaltic transport of a physiological fluid: part I. Flow in non-uniform geometry," *Biorheology*, vol. 20, no. 2, pp. 153–166, 1983.

[20] P. B. Cotton and C. B. Williams, *Practical Gastrointestinal Endoscopy*, Oxford University Press, London, UK, 3rd edition, 1990.

[21] A. E. H. Abd El Naby and A. E. M. El Misiery, "Effects of an endoscope and generalized Newtonian fluid on peristaltic motion," *Applied Mathematics and Computation*, vol. 128, no. 1, pp. 19–35, 2002.

[22] I. Dapra and G. Scarpi, "Perturbation solution for pulsatile flow of a non-Newtonian Williamson fluid in a rock fracture," *International Journal of Rock Mechanics and Mining Sciences*, vol. 44, no. 2, pp. 271–278, 2007.

[23] R. L. Burden and J. D. Faires, *Numerical Analysis*, PWS Publishing Company, Boston, Mass, USA, 5th edition, 1985.